Location Based Beamforming in 5G Ultra-Dense Networks

Petteri Kela*†, Mário Costa*, Jussi Turkka‡, Mike Koivisto§, Janis Werner§, Aki Hakkarainen§
Mikko Valkama§, Riku Jäntti†, and Kari Leppänen*
*Huawei Technologies Oy (Finland). Co. Ltd., Helsinki, Finland
Email: {petteri.kela, mariocosta, kari.leppanen}@huawei.com
†Department of Communications and Networking, Aalto University, Espoo, Finland
Email: riku.jantti@aalto.fi
‡Magister Solutions Ltd., Jyväskylä, Finland
Email: jussi.turkka@magister.fi
§Department of Electronics and Communications Engineering, Tampere University of Technology, Finland
Email: {mike.koivisto, janis.werner, aki.hakkarainen, mikko.e.valkama}@tut.fi

***Abstract*—In this paper we consider transmit (Tx) and receive (Rx) beamforming schemes based on the location of the device. In particular, we propose a design methodology for the Tx/Rx beamforming weight-vectors that is based on the departure and arrival angles of the line-of-sight (LoS) path between access-nodes (ANds) and user-nodes (UNds). A network-centric extended Kalman filter (EKF) is also proposed for estimating and tracking the directional parameters needed for designing the Tx and Rx beamforming weights. The proposed approach is particularly useful in 5G ultra-dense networks (UDNs) since the high-probability of LoS condition makes it possible to design geometric beams at both Tx and Rx in order to increase the signal-to-interference-plus-noise ratio (SINR). Moreover, relying on the location of the UNd relative to the ANds makes it possible to replace full-band uplink (UL) reference signals, commonly employed for acquiring the channel-state-information-at-transmitter (CSIT) in time-division-duplex (TDD) systems, by narrowband UL pilots. Also, employing the EKF for tracking the double-directional parameters of the LoS-path allows one to reduce the rate at which UL reference signals are transmitted. Consequently, savings in terms of time-frequency resources are achieved compared to beamforming schemes based on full-band CSI. Extensive numerical results are included using a realistic ray-tracing based system-level simulator in ultra-dense 5G network context. Results show that position based beamforming schemes outperform those based on full-band CSI in terms of mean user-throughput even for highly mobile users.**

I. Introduction

An explosive growth in the density of wireless cellular devices is expected during the next $5-10$ years. For example, the Next Generation Mobile Networks (NGMN) Alliance has proposed that 5G should support $200-2500$ connections within a square-kilometer with 750Gbps/km^2 area throughput and also up to 2000 connected vehicles with 50Mbps per car downlink (DL) connection [1]. Advanced multiantenna techniques, including spatial multiplexing and network densification, have emerged as key technologies to meet such requirements in the near future [2].

Network densification is an effective way of increasing network capacity, including the mean average throughput of highly mobile user nodes (UNds) [3], [4]. Network densification also helps reaching other 5G targets, such as $<$1ms latencies [5], [6]. However, increasing the density of access-nodes (ANds) as well as that of users makes inter-ANd interference a limiting factor to the performance of the network, specially at sub-6GHz. Coordinated multipoint transmission and coordinated beamforming schemes may be employed in order to mitigate inter-ANd interference [7]–[9]. However, the synchronization and backhaul requirements of such schemes increase the complexity and cost of ultra-dense networks (UDNs).

This paper considers the case where both ANds and UNds are equipped with multiantenna transceivers, thus allowing for transmit and receive beamforming schemes to be employed in order to mitigate inter-ANd interference in spatial division multiplexing. Here, the focus is on connected-car in urban environments where the UNds may have velocities of around 50km/h. In particular, we propose a scheme where the relative positions among ANds and UNds are estimated on a sequential manner, and employed for designing position based transmit and receive beamforming weight vectors. An extended Kalman filter (EKF) is proposed for estimating and tracking the (transmit and receive) angles of the line-of-sight (LoS) path needed for designing the beamformers at the ANds and UNds. Such an EKF does not assume any common coordinate system between ANds and UNds, and takes into account possible rotations of the multiantenna transceiver at the UNd. Moreover, the proposed EKF can reuse the time-frequency-spatial resources of the UDN, and further infrastructure is not needed nor required [10], [11].

The proposed geometric (or position based) beamforming scheme is compared to the more conventional approach based on channel-state-information (CSI) at transmitter and receiver by means of extensive numerical results using a realistic ray-tracing channel model. In addition to improved performance in terms of mean user throughput, the proposed position based beamforming scheme is more efficient in terms of time-frequency resources than that based on full-band CSI.

This paper is organized as follows. Section II describes proposed receive beamforming solutions. In Section III, an EKF is proposed for tracking both transmit and receive angles

This work was supported in part by the Finnish Funding Agency for Innovation (Tekes) under the projects "5th Evolution Take of Wireless Communication Networks" (TAKE-5) and "5G Networks and Device Positioning" (http://www.tut.fi/5G/positioning/index.html).

needed for designing the position based beamformers. Section IV describes the realistic simulation tool used for evaluating the proposed geometric beamforming schemes. Section V provides extensive numerical results comparing the proposed positioning based schemes to that based on CSI. Finally, conclusions and future work are given in Section VI.

II. Downlink Transmit and Receive Beamforming for Ultra-Dense Networks

Let $\boldsymbol{w}_{n,j} \in \mathbb{C}^{N_{\mathrm{ANd}}\times 1}$ denote the transmit beamforming weight-vector towards the nth user being served by jth ANd. Such a weight-vector is designed either based on UL reference signals transmitted from a single antenna of the multiantenna transceiver at the UNd or based on the UNd's position relative to the ANd. Channel reciprocity is exploited in the former case. In the latter case, the angles of the LoS paths between UNds and ANds are used for synthesizing a channel matrix that is employed for calculating the transmit beamforming weight-vectors; see the next sections for details and [11] for an algorithm that estimates the UNd position in the network.

The output of the receive beamforming at the nth ($n \in \{1,\ldots,N\}$) scheduled UNd can be written as [12]

$$x_n = \boldsymbol{z}_n^H \boldsymbol{y}_n, \tag{1}$$

where $\boldsymbol{z}_n \in \mathbb{C}^{N_{\mathrm{UNd}}\times 1}$ and $\boldsymbol{y}_n \in \mathbb{C}^{N_{\mathrm{UNd}}\times 1}$ denote the receive beamforming weight-vector and the multichannel output of the multiantenna receiver of the nth UNd, respectively.

DL reference signals need to be employed in case the receive beamforming weights are determined by the UNd. Here, we consider the case where the ANds transmit DL precoded pilots to all scheduled users simultaneously. This is done in order to reduce the overhead due to DL pilots at the cost of introducing pilot pollution. The SIMO channel used for calculating the receive beamforming weights at the nth user is then

$$\tilde{\boldsymbol{h}}_n = \boldsymbol{H}_{n,j} \sum_{i=1}^{N} \boldsymbol{w}_i, \tag{2}$$

where $\boldsymbol{H}_{n,j}$ denotes the MIMO channel matrix between the nth user and a transmitting jth ANd. Transmit precoding vector for ith user is w_i. The receive beamforming weight-vector $\boldsymbol{z}_n$ is then a function of $\tilde{\boldsymbol{h}}_n \in \mathbb{C}^{N_{\mathrm{UNd}}\times 1}$.

In case of position-based receive beamforming, DL pilots are, however, not employed. Instead, the network estimates and tracks the angles needed for designing both transmit and receive beamforming weight-vectors. The directional parameters needed for calculating the receive beamforming weight-vectors are quantized and transmitted to the UNds on a DL control information (DCI) channel.

The signal-to-interference-plus-noise ratio (SINR) experienced by the user n being served by the ANd j ($j \in \{1,\ldots,K\}$) can be expressed as

$$\mathrm{SINR}_n = \frac{P_{n,j}\|\boldsymbol{z}_n^H \boldsymbol{H}_{n,j}\boldsymbol{w}_{n,j}\|^2}{\sum_{i=1,i\neq n}^{N}\sum_{k=1}^{K} P_{i,k}\|\boldsymbol{z}_n^H \boldsymbol{H}_{n,k}\boldsymbol{w}_{i,k}\|^2 + \sigma_n^2}, \tag{3}$$

where $P_{n,j}$ denotes the transmit power for precoder $w_{n,j}$ and σ_n^2 is the variance of the complex-circular zero-mean white Gaussian noise at the nth user.

A. Location based Transmit and Receive Beamforming

Downlink transmit beamforming schemes exploiting the locations of the users relative to the ANd typically employ a synthesized multi-user multiple input single output (MU-MISO) matrix comprising the LoS-paths, only. Let $\vartheta_n \in [0,\,\pi]$ and $\varphi_n \in [0,\,2\pi)$ denote the co-elevation and azimuth angles of the kth user relative to the ANd's coordinate system (the arrival angles of the UL reference signals), respectively. The synthesized MU-MISO matrix employed in this paper is given by

$$\begin{aligned}\tilde{\boldsymbol{H}} = &[\boldsymbol{a}_{\mathrm{ANd}_H}(\vartheta_1,\varphi_1),\ldots,\boldsymbol{a}_{\mathrm{ANd}_H}(\vartheta_N,\varphi_N)]^T \\ &+ [\boldsymbol{a}_{\mathrm{ANd}_V}(\vartheta_1,\varphi_1),\ldots,\boldsymbol{a}_{\mathrm{ANd}_V}(\vartheta_N,\varphi_N)]^T,\end{aligned} \tag{4}$$

where $\boldsymbol{a}_{\mathrm{ANd}_H}(\vartheta,\varphi), \boldsymbol{a}_{\mathrm{ANd}_V}(\vartheta,\varphi) \in \mathbb{C}^{N_{\mathrm{ANd}}\times 1}$ denote the ANd's array responses due to an horizontal and vertical excitation, respectively. Note that (4) assumes equal power allocation for the two polarizations. The matched-filter (MF) precoder employed in this paper is then given by $\boldsymbol{W}_{\mathrm{MF}} = \tilde{\boldsymbol{H}}^H$ while the zero-forcing (ZF) method is $\boldsymbol{W}_{\mathrm{ZF}} = \tilde{\boldsymbol{H}}^\dagger$, where the superscript $\{\cdot\}^\dagger$ denotes the Moore-Penrose pseudo-inverse.

The downlink receive beamforming vectors can be found in a similar fashion by replacing the angles of the users with those of the ANds.

B. Employed 5G Frame Structure and Numerology

The frame structure and related numerology used in this paper is described in [4]. In particular, the transmission time interval (TTI) length is 0.2ms and each TTI has 42 OFDM symbols. In each TTI 1 symbol is dedicated for narrowband UL pilots (also called beacons) and 4 symbols for full-band UL pilots. The narrowband beacons are used for positioning purposes (see Section III) while the full-band UL beacons are employed for acquiring the CSIT. Moreover, the first symbol of the DL data transmission is used for transmitting full-band DL precoded pilots in order to allow the user to calculate the receive beamforming weights.

C. Discussion on Link Adaptation

Receive beamforming can enhance the desired signal and attenuate interfering signals, if properly designed. However, receive beamforming introduces an additional challenge for link adaptation. In particular, the network should be able to estimate the user-experienced SINR before transmission in order to be able to assign an optimal modulation and coding scheme (MCS) for data transmission. In continuous ultra-dense network (C-UDN) where a central controller is responsible for the scheduling decisions, it can be assumed that interfering precoders of at least closest neighbors are well known. However, it is extremely challenging to estimate the gain obtained from the user receive beamforming accurately.

As the effectiveness of outer-loop link adaptation (OLLA) [13] with multi-user multiple input multiple output (MU-MIMO) was earlier questioned in [5], OLLA algorithm is not expected to work well if transmission beams are formed dynamically on every TTI for mobile users. Due to changing scheduling decisions causing changing radiation patterns of interferers every TTI supplemented with rather rapid channel aging, learning algorithms may lag behind. However, when leakage from closest neighbors is known and receive beamforming is utilized, OLLA can be used for fine-tuning link

adaptation behavior towards a desired block error rate (BLER) target and learning the achievable gain from receive filter utilized by individual user. This is the approach taken in this work.

III. Tracking of Directional Parameters

In this section, we propose an EKF for tracking the directional parameters needed in designing both the transmit and receive position based beamforming weight vectors. The proposed EKF stems from the work in [14]. However, the EKF proposed herein is based on the concentrated log-likelihood function of the radio channel parameters wrt the path weights [15]. Hence, it is more attractive from a computational viewpoint than that in [14] since only the double-directional parameters of the LoS path are tracked. Such an approach is appropriate for designing transmit and receive beamforming weight vectors based on the relative positions between UNds and ANds, given that they are in LoS condition. In fact, the LoS probability in UDNs is typically higher than 0.8 [4]. Such a result follows from the typical inter-site-distance (ISD) of 50m commonly used in UDNs as well as the well-known model for the LoS probability in geometry-based stochastic channel models [16], [17]. We note that the LoS/NLoS condition of a UNd-ANd link may be determined based on the Rice factor of the received signal strength, for example [18]. Next, we propose a network-centric approach where both departure and arrival angles are estimated and tracked by the network. A decentralized approach where the ANd and UNd track the departure of arrival angles of the LoS path independently follows in a straightforward manner from the EKF proposed next.

A. Network-centric Approach

In the network-centric approach the ANds estimate and track the directional parameters for designing the transmit and receive beamforming weight vectors. A DL control channel is then required in order to share the directional parameters for the receive beamforming weight vector with the UNd. In particular, we rely on similar UL pilot signals (or beacons) that are commonly used in UDNs for acquiring the CSIT [4], [5]. Such UL beacons are designed in a manner that the MIMO channel matrix between a UNd-ANd pair can be estimated at the corresponding ANd. It is important to note that the UL beacons used for CSIT typically span the entire frequency band assigned for DL data transmission while the beacons used for tracking the directional parameters of the LoS-path may be narrowband. Hence, position based beamforming is typically more spectral-efficient than CSIT-based beamforming schemes; see Section V.

Let $\boldsymbol{\theta}[k] \in \mathbb{R}^{8\times 1}$ be the state-vector at time-instant k. The state-vector is given by $\boldsymbol{\theta}[k] = [\boldsymbol{\mu}^T[k], \Delta\boldsymbol{\mu}^T[k]]^T$ where $\boldsymbol{\mu}[k] = [\vartheta_{\mathrm{ANd}}[k], \varphi_{\mathrm{ANd}}[k], \vartheta_{\mathrm{UNd}}[k], \varphi_{\mathrm{UNd}}[k]]^T$ and the corresponding rate-of-change parameters are given in $\Delta\boldsymbol{\mu}[k] = [\Delta\vartheta_{\mathrm{ANd}}[k], \Delta\varphi_{\mathrm{ANd}}[k], \Delta\vartheta_{\mathrm{UNd}}[k], \Delta\varphi_{\mathrm{UNd}}[k]]^T$. Here, the co-elevation and azimuth angles at the ANd (the arrival angles of the UL beacons) are denoted by $\vartheta_{\mathrm{ANd}} \in [0,\, \pi]$ and $\varphi_{\mathrm{ANd}} \in [0,\, 2\pi)$, respectively. The corresponding angles at the UNd (the departure angles of the UL beacons) are denoted by $\vartheta_{\mathrm{UNd}} \in [0,\, \pi]$ and $\varphi_{\mathrm{UNd}} \in [0,\, 2\pi)$, respectively.

It is important to note that the angles at the ANd and UNd are given wrt local coordinate systems. Hence, $\vartheta_{\mathrm{ANd}} \neq \pi - \vartheta_{\mathrm{UNd}}$ and $\varphi_{\mathrm{ANd}} \neq \varphi_{\mathrm{UNd}} + \pi$, unlike when the ANd and UNd share a common coordinate system. In particular, the local coordinate systems are defined by the calibration measurement of the antenna arrays at the ANd and UNd. Hence, the network-centric approach considered here requires that the calibration data of the UNd is acquired by the ANd using an UL control channel. In this paper, the calibration data of the ANd and UNd are represented by the corresponding effective aperture distribution functions (EADFs) [15], [19]:

$$\boldsymbol{G}_{\mathrm{ANd}} = [\boldsymbol{G}_{\mathrm{ANd}_H},\, \boldsymbol{G}_{\mathrm{ANd}_V}] \tag{5}$$

$$\boldsymbol{G}_{\mathrm{UNd}} = [\boldsymbol{G}_{\mathrm{UNd}_H},\, \boldsymbol{G}_{\mathrm{UNd}_V}], \tag{6}$$

where the subscripts $\{\cdot\}_H$ and $\{\cdot\}_V$ denote the array responses due to horizontal and vertical excitations.

We consider the so-called information-form of the EKF where the *observed* Fisher-information matrix is employed instead of the approach based on Kalman-gain matrix [20]. This is achieved by employing the matrix-inversion lemma to the Kalman-gain expression. The information-form of the EKF is computationally more efficient than that based on the Kalman-gain when the dimension of the state-vector is smaller than that of the measurement-vector. In particular, the prediction equations of the EKF are given by

$$\boldsymbol{\theta}^-[k] = \boldsymbol{F}\boldsymbol{\theta}[k-1] \tag{7}$$

$$\boldsymbol{P}^-[k] = \boldsymbol{F}\boldsymbol{P}[k-1]\boldsymbol{F}^T + \boldsymbol{Q}[k-1], \tag{8}$$

where $\boldsymbol{F} \in \mathbb{R}^{8\times 8}$, $\boldsymbol{P} \in \mathbb{R}^{8\times 8}$ and $\boldsymbol{Q} \in \mathbb{R}^{8\times 8}$ denote the state-transition matrix, state covariance matrix and state-noise covariance matrix, respectively. Both $\boldsymbol{F}$ and $\boldsymbol{Q}$ can be found from [21, Ch.2] by noting that we have employed a continuous white-noise acceleration model for the state-dynamics. The update equations of the EKF are given by

$$\boldsymbol{P}[k] = \left(\left(\boldsymbol{P}^-[k]\right)^{-1} + \boldsymbol{\mathcal{J}}\left(\boldsymbol{\theta}^-[k]\right)\right)^{-1} \tag{9}$$

$$\Delta\boldsymbol{\theta}[k] = \boldsymbol{P}[k]\,\boldsymbol{v}\left(\boldsymbol{\theta}^-[k]\right) \tag{10}$$

$$\boldsymbol{\theta}[k] = \boldsymbol{\theta}^-[k] + \Delta\boldsymbol{\theta}^-[k], \tag{11}$$

where $\boldsymbol{\mathcal{J}}\left(\boldsymbol{\theta}^-[k]\right)) \in \mathbb{C}^{8\times 8}$ and $\boldsymbol{v}\left(\boldsymbol{\theta}^-[k]\right) \in \mathbb{R}^{8\times 1}$ denote the observed Fisher-information matrix (FIM) of the state-vector and corresponding score-function, respectively. They are found by employing the double-directional radio channel model for the MIMO channel matrix using a single path (the LoS-path) [15], and concentrating the corresponding log-likelihood function wrt the path-weights [22]. In particular, the observed FIM and score-function are given by

$$\boldsymbol{\mathcal{J}}(\boldsymbol{\theta}^-[k]) = \frac{2}{\sigma_h^2}\Re\left\{\left(\frac{\partial \boldsymbol{r}}{\partial \boldsymbol{\theta}^{-T}[k]}\right)^H \frac{\partial \boldsymbol{r}}{\partial \boldsymbol{\theta}^{-T}[k]}\right\} \tag{12}$$

$$\boldsymbol{v}\left(\boldsymbol{\theta}^-[k]\right) = \frac{2}{\sigma_h^2}\Re\left\{\left(\frac{\partial \boldsymbol{r}}{\partial \boldsymbol{\theta}^{-T}[k]}\right)^H \boldsymbol{r}\right\}, \tag{13}$$

where we have assumed a white measurement noise with variance σ_h^2. Moreover, $\boldsymbol{r} = \boldsymbol{\Pi}^{\perp}(\boldsymbol{\theta}^-[k])\boldsymbol{h}[k]$ and $\boldsymbol{\Pi}^{\perp}(\boldsymbol{\theta}^-[k]) = \boldsymbol{I} - \boldsymbol{\Pi}(\boldsymbol{\theta}^-[k])$. Here, $\boldsymbol{h}[k] \in \mathbb{C}^{N_{\mathrm{ANd}}N_{\mathrm{UNd}}\times 1}$ denotes the estimated MIMO channel matrix after employing the $\mathrm{vec}\{\cdot\}$ operation. Moreover, $\boldsymbol{\Pi}(\boldsymbol{\theta}^-[k]) \in \mathbb{C}^{N_{\mathrm{ANd}}N_{\mathrm{UNd}}\times N_{\mathrm{ANd}}N_{\mathrm{UNd}}}$ denotes an orthogonal projection matrix, and it is given by

$\mathbf{\Pi}(\boldsymbol{\theta}^-[k]) = \boldsymbol{A}(\boldsymbol{\theta}^-[k])\boldsymbol{A}^\dagger(\boldsymbol{\theta}^-[k])$. Finally, the MIMO steering matrix is

$$\boldsymbol{A}(\boldsymbol{\theta}^-[k]) = [\boldsymbol{G}_{\mathrm{UNd}_H}, \boldsymbol{G}_{\mathrm{UNd}_V}](\boldsymbol{I}_2 \otimes \boldsymbol{d}(\vartheta_{\mathrm{UNd}}, \varphi_{\mathrm{UNd}})) \otimes [\boldsymbol{G}_{\mathrm{ANd}_H}, \boldsymbol{G}_{\mathrm{ANd}_V}](\boldsymbol{I}_2 \otimes \boldsymbol{d}(\vartheta_{\mathrm{ANd}}, \varphi_{\mathrm{ANd}})), \quad (14)$$

where $\otimes$ denotes the Kronecker product and $\boldsymbol{d}(\vartheta, \varphi)$ denotes a 2-D Fourier vector; see [15], [19] for details where convenient expressions for the derivatives in (12) can also be found.

We note that MIMO channels of practical interest typically comprise many specular and diffuse components; see [15] and Section IV-C. The simplified MIMO channel model used by the EKF proposed in this section is motivated by the typical Rice-factor of $10-20$dBs in UDNs [16], [17], and the computational simplicity of the resulting algorithm. Section V shows by means of extensive numerical results that the proposed EKF has a good tracking performance in realistic channels despite exploiting a simple model for the MIMO radio channel.

B. Initialization of the EKF

The proposed EKF may be initialized as follows. Initial estimates of the state-vector may be found by maximizing the correlation function in [15, Ch.5]. A computationally efficient implementation of such a correlation function based on FFTs is given in [19]. An initial estimate of the state-covariance matrix can be found by evaluating the inverse of the observed FIM at the initial estimate of the state-vector.

IV. Simulation Model

Details of the utilized dynamic 5G time-division-duplex (TDD) system-level simulator are provided in this section. Both UL beaconing and DL are simulated with a TTI resolution. Details of the simulated frame structure can be found in Section II and [4].

A. Simulation Scenario

The scenario considered in this work is the same as that used in [4]. In particular, the simulation map is based on METIS Madrid Grid [23] as illustrated in Fig. 1. On the map 43 ANds are placed in the edges of pavements of vehicular streets. In the highway and pedestrian street, ANds are placed in the middle of the street. The resulting inter-site distances varied from 21.6m to 65m. Table I includes further details on the parameters used in the simulations.

B. Scheduling, Beamforming, Link Adaptation, and Channel Estimation

Used scheduling principles are based on [5]. In simulated C-UDN concept the ANds are assumed to be centrally controlled by an access mobility controllers (AMCs), which take care of handover procedures and information sharing between ANds. Best serving ANd is selected for each user based on beacon measurements. Hence, scheduling of time, frequency and spatial resources for each ANd is done in parallel, but it is assumed that, due to overlapped AMC control areas, interference leakage caused by MU-MIMO precoders of neighboring ANds can be used within interference leakage sharing radius from the perspective of each ANd. Consequently, after scheduling, in the link adaptation phase such interference leakage estimation is used for estimating the SINR of each scheduled user. To learn the gain obtained from receive beamforming, OLLA is used; see Section II. It is assumed that additional delay caused by scheduling and link adaptation is 2 TTIs. Therefore, network cannot use the latest CSI measurements. To mitigate CSI aging and pilot contamination, CSI beacons are scheduled in round robin manner in CSI age order in a way that 250m Euclidean distance between interfering beaconing users is maintained.

TABLE I
Simulation Parameters

Parameter	Value
Simulation scenario	METIS Madrid Grid [23]
Carrier bandwidth	Unpaired 200 MHz
Center frequency	3.5 GHz
Modulation scheme	OFDM
Channel model	METIS map-based model [16]
CSI beacon scheduling	Beacons: round robin in CSI age order with 25m CP compensation distance [5] 250m beacon reuse distance [5]
Data scheduling	MT w/ rate CSI age weighting [5]
Link Adaptation	Inner and outer loop
Traffic model	Infinite buffer
User nodes	1000 per km^2
UNd velocity	0km/h, 50km/h
Network (Synchronous)	43 ANds 20 TX ant./ANd 5m antenna height 4 RX ant./UNd ($\lambda/2$-separation of antennas)
TX array model	Circular array with 3GPP dual-polarized patch antennas [17]
RX array model	Circular array with cross-dipoles
ANd TX power budget	23 dBm
UNd TX power	10 dBm
CSI	Estimated from full-band (CSI) UL beacons using LSE
Position based RBF angles	2 degree static error added to both azimuth and elevation Provided within DCI with integer values
EKF for directional parameters	Using narrowband (single-subcarrier) UL/DL beacons with frequency-hopping

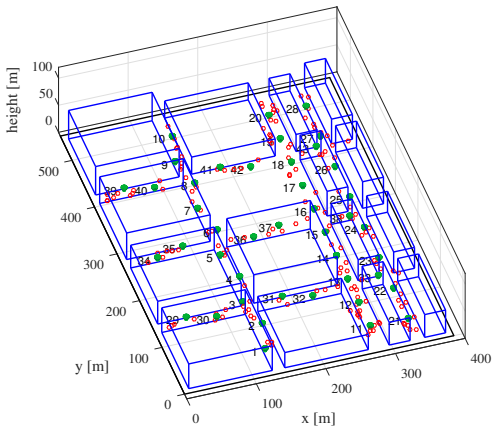

Fig. 1. Considered C-UDN deployment scenario with 43 ANds, illustrated by green dots. ANds are placed at the edges of pavements of ordinary streets. On the pedestrian street and highway ANds are located at the center of the street. Users are illustrated by red circles.

C. Ray Tracing Model

In this study, radio channel characteristics such as pathloss, slow fading and fast fading are modelled using METIS map-

based channel model described in [16]. The model utilizes ray tracing principles using 3D geometric description of the propagation environment and virtually moving random point scatterers. The radio channel between transmitter and receiver is composed of multipath components based on diffractions and reflections. Both the first order and the second order reflections from walls and ground were modeled according to [16]. The diffraction model is based on Berg's model taking into account corner and rooftop diffractions described in [16]. The benefit of a map-based channel model is that it provides spatially consistent channel properties that are needed when MU-MIMO and beamforming techniques are studied together with user mobility. Spatial consistency guarantees that users near each other have similar channel characteristics and small movements do not change channel characteristics significantly. Stochastic channel models, e.g. 3GPP 3D channel model [17], cannot model such effects realistically enough.

The complex polarimetric channel impulse response between receiver antenna element u and transmitter antenna element s with a true motion is given by

$$H_{s,u}(t,\tau) = \sum_{k=1}^{K} \boldsymbol{g}_{u,k}(t)^T \boldsymbol{h}_{k,u,s}(t) e^{\frac{j2\pi d_k(t)}{\lambda}} \boldsymbol{g}_{s,k}(t)\delta(\tau - \tau_{k,u,s}(t)), \quad (15)$$

where variable λ is the wavelength, variable $d_k(t)$ is the total distance of kth multipath in meters at time t and variable K is the total number of multipath components. Vectors $\boldsymbol{g}_{u,k}$ and $\boldsymbol{g}_{s,k}$ are polarimetric antenna patterns of the receiver element u and transmitter element s. The 2×1 pattern vectors contain antenna patterns for vertically and horizontally polarized fields depending on the used frequency and the corresponding arrival and departure angles for azimuth and elevation direction of the kth multipath component at time t. The 2×2 polarization matrix $\boldsymbol{h}_{u,s,k}$ is an element-wise product of path segment matrices $\boldsymbol{h}_{k,i,u,s}$ given by

$$\boldsymbol{h}_{k,u,s}(t) = \frac{\lambda}{4\pi} \prod_{i=1}^{I_k} h_{k,i,u,s}(t) F_{u,s}^{k,i}. \quad (16)$$

The 2×2 complex segment matrices contain an additional attenuation from ith interaction (reflection, diffraction or scattering) of the kth multipath component. Variable $\delta(\tau - \tau_{k,u,s}(t))$ is the delta function for impulse response for different multipath delays $\tau_{k,u,s}$ as the channel evolves in time. Divergence factors $F_{u,s}^{k,i}$ are described in [16] for different interaction types. The divergence factor scales the $h_{k,i,u,s}(t)$ according to segment distance e.g., in case of LoS the divergence is $d_{k,i}^{-1}$ which would correspond to free space loss in (16). It is worth noting that if a path contains diffraction then $\boldsymbol{h}_{u,s,k}$ is derived from the Berg's fictitious distance with $F_{u,s}^{k,i}$ being 1.

Virtually moving scatterers are modelled introducing additional multipath specific Doppler shift component ω_k^{obj} for those path segment matrices that involve scattering from moving objects.

$$\boldsymbol{h}_{k,i,u,s}^{obj}(t) = \boldsymbol{h}_{k,i,u,s}(t) e^{jt\omega_k^{obj}} \quad (17)$$

The variable ω_k^{obj} is calculated from the scattering object speed (3 m/s in this study) and angle difference between path azimuth of arrival and scattering object direction of movement (fixed to 0 degrees in this study).

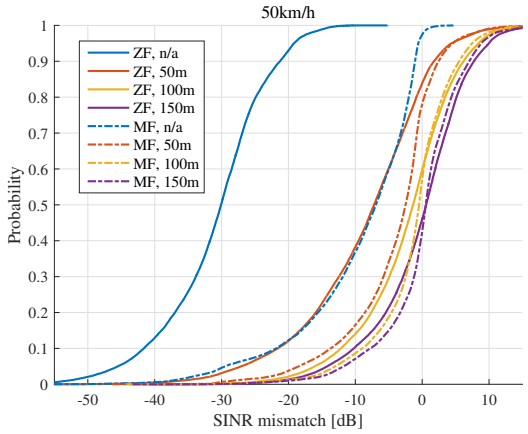

Fig. 2. Cumulative distribution function (CDF) of the SINR mismatch of scheduled users moving 50km/h velocity. Here SINR mismatch refers to the difference between SINR estimation used for link adaptation without OLLA and actual received SINR for different interference leakage information sharing radii.

V. Numerical Results

In this section, reasoning for proposed link adaptation cooperation for UDNs utilizing MU-MIMO is provided. Moreover, results from extensive simulation studies of proposed EKF as well as of the transmit and receive beamforming schemes are provided.

A. Link Adaptation Cooperation

In Fig. 2 SINR mismatches (i.e. difference between estimated and actual SINRs) with zero-forcing (ZF) and matched filter (MF) precoding for different interference leakage sharing radii are shown without OLLA. This study suggests that the close-to-optimal interference information sharing radius is around 100m for considered C-UDN network since in that point the SINR mismatch start to saturate. Further, sensitiveness of dynamic scheduling, especially with ZF, can be seen in a way that if ANd is doing scheduling and link adaptation independently, then link adaptation is not able to estimate SINR properly due to channel aging and varying scheduling decisions for every TTI. Moreover, in case of ZF, precoders formed by single ANd are not expected to interfere with each other. Hence, without adding inter-ANd interference effect, estimation will be too optimistic. Therefore, in rest of the simulation results the close-to-optimal 100m leakage sharing radius is used. Since effect of channel aging and receive beamforming gain cannot be obtained without user measurements and CSI reporting, OLLA is used for fine-tuning SINR estimations further to reach desired 10% BLER target.

B. Performance of the Proposed EKF

Fig. 3 illustrates the performance of the network-centric EKF proposed in Section III. For these results, we considered a UNd moving on the Madrid grid illustrated in Fig. 1 with varying velocity (20 − 50km/h). The coordinate system of the circular array at the UNd is different from that of the ANds by a rotation of 20° in the xy-plane. However, such a mismatch is unknown to the network-centric EKF. Moreover, the orientation of the circular array at the UNd changes according to its route, such as in turns. The departure and arrival angles

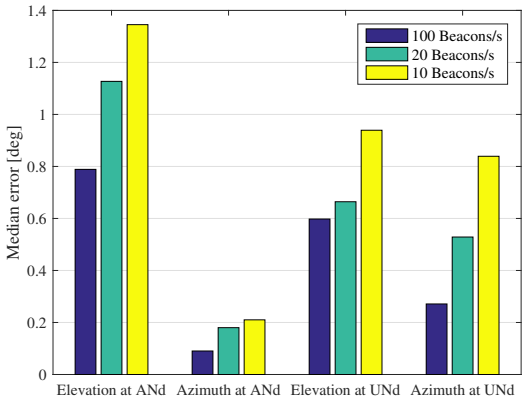

Fig. 3. Performance of proposed EKF in terms of median angular error (in degrees) as a function of the transmission rate of narrowband (single-subcarrier) UL reference signals. An accuracy well below 2° is achievable for all directional parameters.

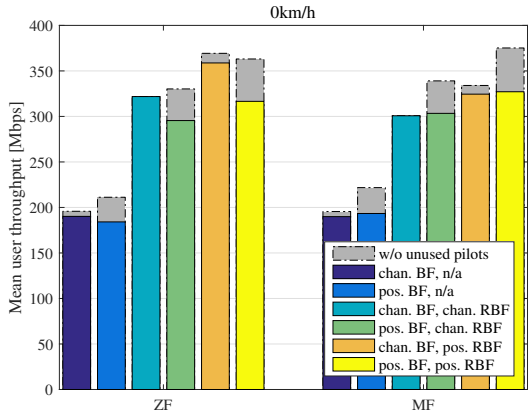

Fig. 4. Performance of CSI and position based beamforming schemes in terms of mean user-throughput with stationary users. Transmit-only beamforming (BF) with a single antenna at the receiver as well as transmit and receive beamforming (RBF) schemes are considered. Effect of utilizing unused wideband DL/UL pilot symbols for data transmission is illustrated with gray color. Position-based receive beamforming schemes outperform those based on DL CSI.

tracked by the proposed EKF are given wrt the coordinate systems of the ANd and UNd, respectively. This follows from using the calibration data of the ANd's and UNd's antenna array. The results in Fig. 3 show that an accuracy well below 2° is achievable for all directional parameters. Hence, in the numerical study given in the next section (Section V-C) we take a conservative approach and employ a fixed angular error of 2° for all directional parameters.

C. Performance of the Proposed Transmit and Receive Beamforming Schemes

Figs. 4 and 5 illustrate the performance of CSI-based and position-based beamforming schemes in terms of mean user-throughput. Stationary users and users moving at 50km/h have been considered. The figures also illustrate the effects due to pilot overhead caused by full-band reference signals needed in CSI-based beamforming schemes. Position-based beamforming schemes do not require full-band reference signals: narrowband (single-subcarrier) pilots suffice.

Results show that the ZF and MF beamforming schemes have similar performance in the considered scenario. This can be explained by the large amount of available degrees-of-freedom at the ANds compared to the amount to served users. For stationary users, the slightly better performance of ZF compared to MF follows from the greater inter-beamformer interference mitigation capability of the former. Results also show that a significant improvement in performance is achieved by employing transmit *and* receive beamforming schemes compared to the transmit-only beamforming case.

Moreover, the results in Figs. 4 and 5 illustrate that position-based receive beamforming schemes outperform those based on full-band CSI. The reason is threefold. Firstly, the EKF makes it possible to design receive beamformers in a way that the corresponding beams are directed towards the dominant LoS path with small angular errors. Secondly, in case of channel based receive beamforming, the precoded DL (full-band) pilots are transmitted simultaneously in order to minimize the control channel capacity. Hence, DL pilot contamination degrades the performance of channel based receive beamforming

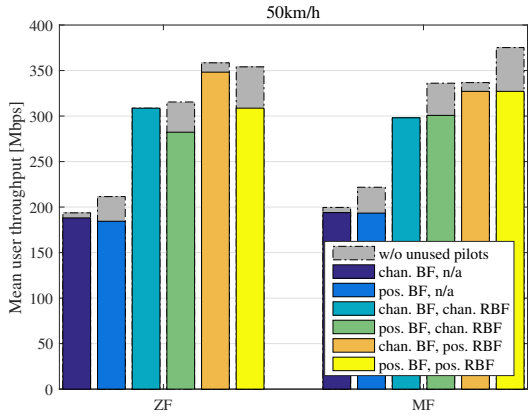

Fig. 5. Performance of CSI and position based beamforming schemes in terms of mean user-throughput with users moving at 50km/h. Transmit-only beamforming (BF) with a single antenna at the receiver as well as transmit and receive beamforming (RBF) schemes are considered. Effect of utilizing unused wideband DL/UL pilot symbols for data transmission is illustrated with gray color. Position-based schemes, especially the MF precoder, were able to maintain their performance without notable loss when compared to the stationary case.

schemes. Finally, in case of transmit beamforming, position based precoding schemes outperform those based on CSI only when the symbols used for acquiring the full-band CSIT are employed for data transmission.

SINR distributions of scheduled users are shown in Fig. 6. It can be seen that rather large gain can be obtained with multi-antenna receiver capable of receive beamforming when compared to single antenna receivers. SINR distribution also shows that with ZF more uniform throughput distribution can be achieved due to better interference cancellation capabilities.

It was observed from simulation results that receive beamforming did not have a significant effect on usage of the available degrees of freedom. However, transmission precoder selection had the effect shown in Fig. 7. In particular, with

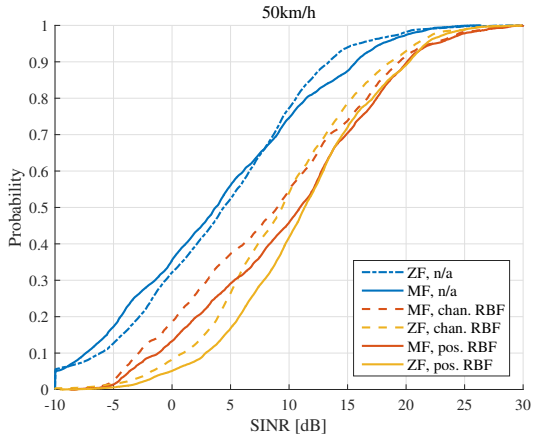

Fig. 6. CDF of the SINR of scheduled users moving at 50km/h and served with CSI-based transmit precoders. Significant gain of receive beamforming compared to single antenna user can be seen. Position based receive beamforming outperforms CSI based throughout the distribution.

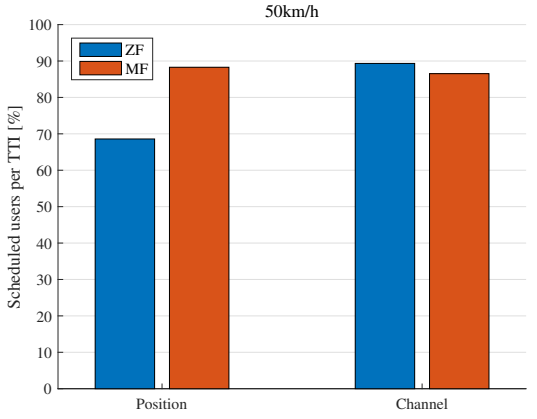

Fig. 7. Percentage of simulated users being scheduled per TTI on average with different transmit precoding schemes. Position information based ZF precoder scheduled $\sim 22\%$ less users per TTI than the MF precoder.

position based transmit precoders utilizing ZF precoding $\sim 22\%$ fewer users were able to schedule successfully. Since network was tracking user positions, also serving ANd was selected based on Euclidean distance between user and ANd. Hence, regardless of high probability of LoS connection, Los condition is not quaranteed in such distance based association process. Due to this some users were in non-LoS position to serving ANd. Therefore it was more probable with error sensitive ZF precoding, that the received SINR was insufficient even for the lowest MCS, if user was around the corner and precoder was designed only for LoS path.

VI. Conclusions and Future Work

Transmit and receive beamforming can greatly improve the performance of UDNs. Estimating and tracking the location of the users relative to the ANds, and employing such directional parameters for designing the beamforming weights was shown to be an effective solution for improving the mean user-throughputs, given that a LoS condition is available. Such improvements are particularly relevant since the overhead due to full-band UL reference signals on the frame structure can be reduced significantly.

The proposed position based beamforming scheme is also expected to provide improvements to the battery consumption of the user devices compared to traditional approaches that are based on full-band UL pilots. This is due to the employed narrowband UL reference signals and the possibility of tracking the directional parameters needed for designing the beamforming weights. Finally, position based beamforming schemes may also be used for increasing the control channel capacity by sending dedicated control information to spatially separated users.

References

[1] NGMN Alliance, "5G White Paper," 2015. [Online]. Available: http:/www.ngmn.org/5g-white-paper/

[2] Huawei Technologies, "5G: New air interface and radio access virtualization," 2015. [Online]. Available: http://www.huawei.com/minisite/has2015/img/5g_radio_whitepaper.pdf

[3] X. Gelabert, P. Legg, and C. Qvarfordt, "Small cell densification requirements in high capacity future cellular networks," in *2013 IEEE ICC Workshops (ICC)*, June 2013, pp. 1112–1116.

[4] P. Kela et al., "Supporting mobility in 5G: A comparison between massive MIMO and continuous ultra dense networks," in *accepted for publication in Proc. IEEE International Conference on Communications (ICC)*, May 2016.

[5] P. Kela, J. Turkka, and M. Costa, "Borderless mobility in 5G outdoor ultra-dense networks," *IEEE Access*, vol. 3, pp. 1462–1476, September 2015.

[6] P. Kela et al., "A novel radio frame structure for 5G dense outdoor radio access networks," in *IEEE 81st Vehicular Technology Conference (VTC2015-Spring)*, May 2015.

[7] H. Dahrouj and W. Yu, "Coordinated beamforming for the multicell multi-antenna wireless system," *IEEE Transactions on Wireless Communications*, vol. 9, no. 5, pp. 1748–1759, May 2010.

[8] D. Lee et al., "Coordinated multipoint transmission and reception in LTE-advanced: Deployment scenarios and operational challenges," *IEEE Communications Magazine*, vol. 50, no. 2, pp. 148–155, February 2010.

[9] D. Gesberg et al., "Multi-cell MIMO cooperative networks: A new look at interference," *IEEE Journal on Selected Areas in Communications*, vol. 28, no. 9, pp. 1380–1408, December 2010.

[10] A. Dammann, R. Raulefs, and S. Zhang, "On prospects of positioning in 5G," in *2015 IEEE ICC Workshops (ICC)*, June 2015.

[11] J. Werner et. al, "Joint user node positioning and clock offset estimation in 5G ultra-dense networks," in *Proc. IEEE Global Communications Conference (GLOBECOM)*, Dec 2015.

[12] A. B. Gershman et al., "Convex optimization-based beamforming," *IEEE Signal Process. Mag.*, vol. 27, no. 3, pp. 62–75, May 2015.

[13] K. Pedersen et al., "Frequency domain scheduling for OFDMA with limited and noisy channel feedback," in *IEEE 66th Vehicular Technology Conference (VTC2015-Fall)*, September 2007.

[14] J. Salmi, A. Richter, and V. Koivunen, "Detection and tracking of MIMO propagation path parameters using state-space approach," *IEEE Transactions on Signal Processing*, vol. 57, no. 4, pp. 1538–1550, April 2009.

[15] A. Richter, "Estimation of radio channel parameters: Models and algorithms," Ph.D. dissertation, Ilmenau University of Technology, 2005.

[16] METIS, "D1.4 channel models," 2014. [Online]. Available: https://www.metis2020.com

[17] 3GPP TR 36.873, "Study on 3D channel model for LTE (release 12)," June 2015. [Online]. Available: http://www.3gpp.org

[18] F. Benedetto, G. Giunta, A. Toscano, and L. Vegni, "Dynamic LOS/NLOS statistical discrimination of wireless mobile channels," in *Proc. Vehicular Technology Conference (VTC)*, 2007, pp. 3071–3075.

[19] M. Costa, A. Richter, and V. Koivunen, "DoA and polarization estimation for arbitrary array configurations," *IEEE Transactions on Signal Processing*, vol. 60, no. 5, pp. 2330–2343, May 2012.

[20] Y. Bar-Shalom, X. Li, and T. Kirubarajan, *Estimation with Applications to Tracking and Navigation*. John Wiley & Sons, Inc., 2001.

[21] J. Hartikainen, A. Solin, and S. Särkkä, "Optimal filtering with Kalman filters and smoothers," 2011. [Online]. Available: http://becs.aalto.fi/en/research/bayes/ekfukf/documentation.pdf

[22] M. Viberg, B. Ottersten, and T. Kailath, "Detection and estimation in sensor arrays using weighted subspace fitting," *IEEE Transactions on Signal Processing*, vol. 39, no. 11, pp. 2436–2449, November 1991.

[23] METIS, "Scenarios, requirements and KPIs for 5G mobile and wireless system," 2013. [Online]. Available: https://www.metis2020.com